

# A relationship between the aerodynamic and physical roughness of winter sea ice

Edgar L Andreas\*

NorthWest Research Associates, Inc., Lebanon, New Hampshire, USA

\*Correspondence to: E. L Andreas, NorthWest Research Associates, Inc. (Seattle Division), 25 Eagle Ridge, Lebanon, New Hampshire, 03766-1900, United States, 603-448-3555. E-mail: eandreas@nwra.com

A bulk flux algorithm predicts the turbulent surface fluxes of momentum and sensible and latent heat from mean measured or modelled meteorological variables. The bulk flux algorithm resulting from data collected over winter sea ice during SHEBA, the experiment to study the Surface Heat Budget of the Arctic Ocean, failed, however, in its first trial to predict the turbulent momentum flux over sea ice in the Antarctic. This result suggests that the main parameter for predicting the momentum flux, the aerodynamic roughness length  $z_0$ , does not respond just to the friction velocity, as in the SHEBA algorithm, but is closely related to the physical roughness of snow-covered sea ice and may need to be site-specific. I investigate this idea with simultaneous measurements of  $z_0$  and the physical roughness of the surface,  $\xi$ , at Ice Station Weddell. The metric  $\xi$  derives from surveys of surface elevation and is related to but always less than the standard deviation in surface elevation. On combining the  $z_0$ – $\xi$  pairs from Ice Station Weddell with similar data obtained over Arctic sea ice, I show that the Arctic and Antarctic  $z_0$ – $\xi$  data lie along a continuum such that measuring  $\xi$  could provide a means for estimating a site-specific  $z_0$  for any global sea ice surface. Backscatter data from satellite-borne synthetic aperture radar might provide a remotely sensed estimate of  $\xi$ . Copyright © 2011 Royal Meteorological Society

**Key Words:** bulk turbulent flux algorithm; drag coefficient; Ice Station Weddell; roughness length; SHEBA; snow; turbulence measurements

Received 12 August 2010; Revised 1 February 2011; Accepted 12 April 2011; Published online in Wiley Online Library 15 June 2011

**Citation:** Andreas EL. 2011. A relationship between the aerodynamic and physical roughness of winter sea ice. *Q. J. R. Meteorol. Soc.* **137**: 1581–1588. DOI:10.1002/qj.842

## 1. Introduction

During SHEBA, the 1997–1998 experiment to study the Surface Heat Budget of the Arctic Ocean, the Atmospheric Surface Flux Group measured the turbulent surface fluxes of momentum and heat hourly at multiple sites over sea ice for almost a year (Andreas *et al.*, 1999). We presumed that a bulk turbulent surface flux algorithm obtained from such a large dataset (i.e. Andreas *et al.*, 2010a, 2010b), which featured measurements in all seasons and over several ice types, would be accurate over any oceanic sea ice surface. Our first test of this hypothesis was disappointing.

Figure 1 shows tests of our algorithm (i.e. Andreas *et al.*, 2010b) in predicting the surface momentum flux over winter sea ice at one of our SHEBA sites and for comparable measurements on Ice Station Weddell, in the Antarctic. By winter sea ice, I mean ice that is compact and snow-covered, and the snow is dry and cold enough to drift and blow under wind forcing (Andreas *et al.*, 2010a, 2010b). In Figure 1, I use the friction velocity,  $u_*$ , as a surrogate for the momentum flux.

Figure 1 shows that the SHEBA bulk flux algorithm does well in replicating the values of  $u_*$  measured hourly by eddy covariance at SHEBA Flux-PAM (for portable automated mesonet) site 'Baltimore'. The comparison is similarly good

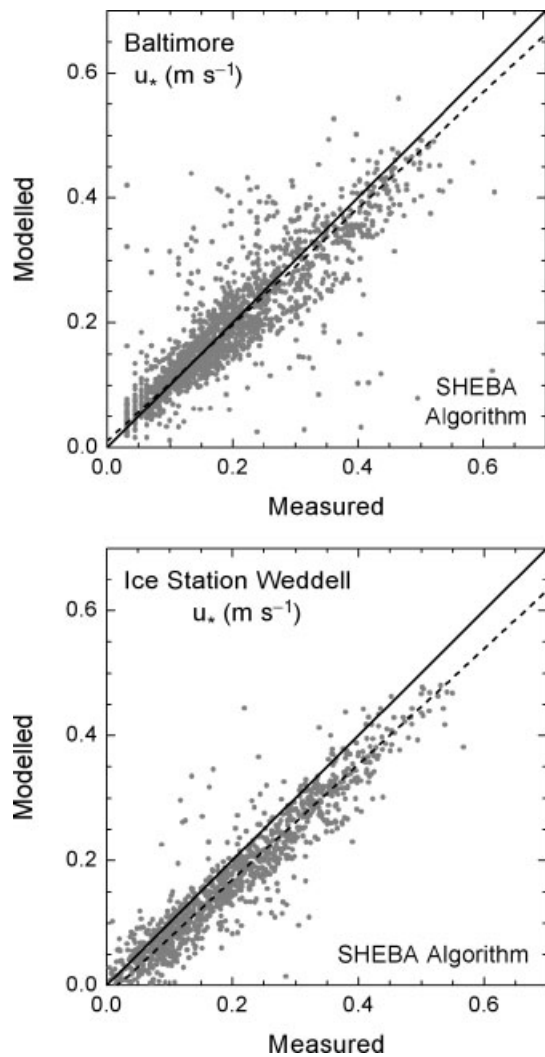


**Figure 1.** The SHEBA bulk flux algorithm for winter (Andreas *et al.*, 2010b) is used to predict the friction velocity,  $u_*$ , for the SHEBA Flux-PAM (for portable automated mesonet) site called ‘Baltimore’ and for Ice Station Weddell. The panels show those ‘modelled’  $u_*$  values compared with hourly measurements of  $u_*$  by eddy covariance (Andreas *et al.*, 2005, 2010b). The solid line is 1:1; the dashed line is the best fit through the data, computed as the bisector of  $y$ -versus- $x$  and  $x$ -versus- $y$  least-squares fits.

for other SHEBA sites (Andreas *et al.*, 2010b). For the Antarctic data from Ice Station Weddell (Andreas *et al.*, 2004, 2005), on the other hand, the modelled  $u_*$  values are, on average, biased low by about  $0.03 \text{ m s}^{-1}$ . Such a bias is not tolerable in sea ice, climate, and weather forecasting models for which our algorithm is intended. Such a low bias would affect estimates of ice thickness, among other quantities, by reducing ridging and by biasing the turbulent surface heat fluxes. We therefore need to understand why this bias occurs.

Shortly, I will describe the data and explain the details of the algorithm used in creating Figure 1. For now, though, I just present these results as evidence that all sea ice sites are not aerodynamically similar, even if they are visually similar. A ‘universal’ bulk turbulent flux algorithm may need to be more site-specific than Andreas *et al.* (2010b) assumed.

In this paper, I therefore focus on predicting momentum exchange over winter sea ice with a bulk flux algorithm. Predicting the surface fluxes of sensible and latent heat is also a requirement of a bulk flux algorithm, but we first need to sort out these problems in predicting  $u_*$  before we can

judge the need for improving predictions of the turbulent heat fluxes.

On Ice Station Weddell, we measured the physical roughness of the surface; and I here relate that roughness metric to the aerodynamic roughness,  $z_0$ , required in bulk flux algorithms. This Ice Station Weddell dataset is consistent with but over three times larger than the only similar previous analysis – by Banke *et al.* (1980) for Arctic sea ice. Combining the Ice Station Weddell and Banke *et al.* datasets is a first step in connecting the aerodynamic roughness to the site-specific physical roughness of a sea ice surface.

## 2. Bulk flux algorithm

Andreas *et al.* (2010a, 2010b) give the full details of the SHEBA bulk turbulent flux algorithms for summer and winter sea ice that I used to create Figure 1. Hence, here I will discuss only the basic equations.

Bulk flux algorithms (cf. Fairall *et al.*, 1996, 2003) are used for estimating the turbulent surface fluxes of momentum ( $\tau$ , also called the surface stress) and sensible ( $H_s$ ) and latent ( $H_L$ ) heat in analyses and models. The main equations are based on Monin–Obukhov similarity theory and take the forms (e.g. Garratt, 1992, pp 52 ff)

$$\tau \equiv \rho u_*^2 = \rho C_{Dr} S_r^2, \quad (2.1a)$$

$$H_s = \rho c_p C_{Hr} S_r (\Theta_s - \Theta_r), \quad (2.1b)$$

$$H_L = \rho L_s C_{Er} S_r (Q_s - Q_r). \quad (2.1c)$$

Here,  $\rho$  is the air density;  $c_p$  is the specific heat of air at constant pressure;  $L_s$  is the latent heat of sublimation;  $S_r$  is an effective wind speed at reference height  $r$ ;  $\Theta_r$  and  $Q_r$  are the potential temperature and specific humidity, respectively, at height  $r$ ; and  $\Theta_s$  and  $Q_s$  are the temperature and specific humidity at the surface. Because the surface is snow or ice, I evaluate  $Q_s$  as the saturation value at temperature  $\Theta_s$ . Equation (2.1a) also defines the friction velocity,  $u_*$ , which I use instead of  $\tau$  to quantify the surface stress.

The essence of any bulk flux algorithm is how it evaluates the transfer coefficients for momentum, sensible heat, and latent heat appropriate for reference height  $r$ : respectively,  $C_{Dr}$ ,  $C_{Hr}$ , and  $C_{Er}$  in (2.1). These derive from Monin–Obukhov similarity theory and formally are

$$C_{Dr} = \frac{k^2}{\{\ln(r/z_0) - \psi_m(r/L)\}^2}, \quad (2.2a)$$

$$C_{Hr} = \frac{k^2}{\{\ln(r/z_0) - \psi_m(r/L)\} \{\ln(r/z_T) - \psi_h(r/L)\}}, \quad (2.2b)$$

$$C_{Er} = \frac{k^2}{\{\ln(r/z_0) - \psi_m(r/L)\} \{\ln(r/z_Q) - \psi_h(r/L)\}}. \quad (2.2c)$$

In these equations,  $k$  ( $= 0.40$ ) is the von Kármán constant, and  $\psi_m$  and  $\psi_h$  are empirical functions of the Obukhov length

$$L = -\frac{\bar{\Theta}}{kg} \left( \frac{u_*^3}{(H_s/\rho c_p) + \frac{0.61\bar{\Theta}}{1+0.61Q}(H_L/\rho L_s)} \right). \quad (2.3)$$

Here,  $g$  is the acceleration of gravity, and  $\overline{\Theta}$  and  $\overline{Q}$  are surface-layer averages of the air temperature and specific humidity.

Andreas *et al.* (2010a, 2010b; cf. Fairall *et al.*, 1996, 2003; Andreas *et al.*, 2008) explain that  $S_r$  in (2.1) is not just the measured or modelled wind speed but also includes a parametrization for gustiness. Andreas *et al.* (2010a, 2010b) also describe how the SHEBA algorithms parametrize  $z_0$ ,  $z_T$ ,  $z_Q$ ,  $\psi_m$ , and  $\psi_h$ . As with most bulk flux algorithms, (2.1) and (2.2) are coupled through the Obukhov length, (2.3), and therefore must be solved iteratively.

Because  $z_0$  is the key variable for estimating  $u_*$  (i.e. see (2.1a) and (2.2a)) and because this aerodynamic roughness is the variable most closely associated with the physical roughness of a surface (Lettau, 1969; Arya, 1975; Banke *et al.*, 1980; Raupach, 1992; Andreas, 1995; Shao and Yang, 2005), I focus on parametrizing it in this paper.

The SHEBA parametrization for  $z_0$  in winter – the parametrization that I used to create both panels in Figure 1 – is (Andreas *et al.*, 2010b)

$$z_0 = 0.135 \frac{\nu}{u_*} + B \tanh^3(13u_*). \quad (2.4)$$

Here,  $z_0$  is in metres,  $u_*$  is in  $\text{m s}^{-1}$ ,  $\nu$  is the kinematic viscosity of air in  $\text{m}^2 \text{s}^{-1}$ , and  $B = 2.3 \times 10^{-4}$  m. The first term on the right in (2.4) models the aerodynamically smooth regime; the second term treats aerodynamically rough flow and the transition from smooth to rough flow.

If I had increased  $B$  in (2.4) to  $6.0 \times 10^{-4}$  m, the modelled  $u_*$  values in the Ice Station Weddell panel in Figure 1 would have fallen much closer to the 1:1 line. Therefore, Figure 1 and (2.4) imply that the sea ice at Ice Station Weddell was generally more aerodynamically rough than the ice at SHEBA.

### 3. Turbulence data

Ice Station Weddell drifted from early February through to early June 1992 in the western Weddell Sea, paralleling the track of Shackleton's *Endurance*. Andreas and Claffey (1995) and Andreas *et al.* (2004, 2005) give full details of the mean and turbulence data collected on Ice Station Weddell.

Briefly, the turbulence data relevant to this paper came from a sonic anemometer/thermometer and a Lyman-alpha hygrometer mounted on a tower at a height of 4.65 m and sampled at 10 Hz. The turbulent fluxes were averaged hourly and calculated as covariances. That is,

$$\tau = -\rho \overline{uw}, \quad (3.1a)$$

$$H_s = \rho c_p \overline{w\theta}, \quad (3.1b)$$

$$H_L = \rho L_s \overline{wq}. \quad (3.1c)$$

Here,  $u$ ,  $w$ ,  $\theta$ , and  $q$  are turbulent fluctuations in longitudinal velocity, vertical velocity, temperature, and specific humidity; the overbar indicates an hour of averaging.

I did the usual coordinate rotations to align  $\overline{uw}$  with the mean wind and made a Webb correction to  $H_L$ . The turbulence measurements ran continuously from late February through to late May 1992; I excluded data, though, when the air flow was disturbed by structures on Ice Station Weddell. The surface at Ice Station Weddell was compact, second-year sea ice with a snow cover typically 0.4–0.5 m deep.

Although section 2 described our so-called SHEBA bulk flux algorithm, the only SHEBA data I use here are from the Flux-PAM site called 'Baltimore' that I already showed in Figure 1. As brief background for this figure, the SHEBA ice camp drifted in the Beaufort Gyre from early October 1997 until early October 1998. The SHEBA Flux-PAM stations (Militzer *et al.*, 1995; Horst *et al.*, 1997) measured  $\tau$  and  $H_s$  hourly with a sonic anemometer/thermometer at a single height that ranged between 2.3 and 3.5 m above the surface. The fluxes were processed as eddy covariances, as on Ice Station Weddell. See Persson *et al.* (2002) and Andreas *et al.* (2010a, 2010b) for more details about the SHEBA measurements.

Andreas *et al.* (2010a, 2010b; cf. Brunke *et al.*, 2006) divided the SHEBA year into just two aerodynamic seasons, winter and summer, on the basis of ice conditions. In 'winter', the sea ice was compact and continuously snow-covered, and the snow was dry enough to drift and blow. In 'summer', the snow became too wet and sticky to drift and eventually disappeared entirely at the SHEBA camp to expose bare sea ice. In this paper, because I concentrate on measurements from Ice Station Weddell, which was a 'winter' deployment, the 'Baltimore' data in Figure 1 are for just the SHEBA winter. During SHEBA, winter ran from the beginning of the measurements in late October 1997 through to 14 May 1998. It resumed on 15 September 1998 and continued through to the end of September, when we began closing the SHEBA camp.

From the Ice Station Weddell data, I evaluated  $z_0$  from (2.1a) and (2.2a) as

$$z_0 = r \exp \left[ - \left\{ k C_{Dr}^{-1/2} + \psi_m(r/L) \right\} \right], \quad (3.2)$$

where  $z_0$  and  $r$  are in metres. All quantities on the right here were measured or otherwise known. In particular, for  $\psi_m$ , I used the function from Paulson (1970) in unstable stratification and the function from Grachev *et al.* (2007) in stable stratification. I screened the resulting hourly values and discounted four cases for which  $z_0 \geq 0.1$  m. Computed values of  $z_0$  this large over compact, snow-covered ice are obviously erroneous (e.g. Banke *et al.*, 1980; Overland, 1985; Guest and Davidson, 1991; Andreas, 1995).

After finding  $z_0$  from (3.2), I could also calculate the drag coefficient for neutral stability at a standard reference height of 10 m from (2.2a) as

$$C_{DN10} = \left\{ \frac{k}{\ln(10/z_0)} \right\}^2. \quad (3.3)$$

This and  $z_0$  are interchangeable quantities for characterizing the aerodynamic properties of a surface.

### 4. The physical roughness of sea ice

Banke *et al.* (1980; also Banke and Smith, 1973; Banke *et al.*, 1976) pioneered attempts to relate the aerodynamic roughness of sea ice,  $z_0$ , to the physical roughness. At several Arctic sites, they measured profiles of surface elevation,  $h$ , along lines upwind of their sonic anemometer using a transit and levelling rod. The profile lines were typically 256 m long, and the sampling interval was 1–2 m.

On taking the Fourier transform of the  $h$  series, Banke *et al.* (1980) obtained the wave-number spectrum of the elevation,  $\Phi(\kappa)$ , where  $\kappa$  is the wave number. In turn, they

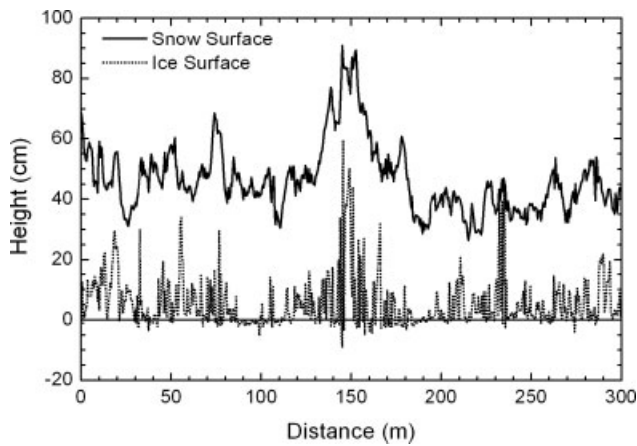


**Figure 2.** Typical levelling survey of the snow and sea ice surfaces on Ice Station Weddell on Julian day 78 in 1992. The roughness parameter for the snow surface profile here,  $\xi$ , obtained from (4.1), is 3.72 cm. The horizontal line at 0 cm on the vertical axis is sea level.

integrated this spectrum to obtain  $\xi$ , a metric for the physical roughness of the snow surface in the along-wind direction:

$$\xi^2 = \int_{\kappa_0}^{\infty} \Phi(\kappa) d\kappa. \quad (4.1)$$

Here,  $\kappa_0 = 0.5 \text{ m}^{-1}$  is the lower limit of the integration and corresponds to a maximum wavelength in this integration of 12.6 m.

Banke *et al.* (1980) imposed this lower limit of integration in (4.1) under the assumption that features with wavelengths longer than 12.6 m ‘appear streamlined to the wind’ and, thus, have no role in air–surface momentum exchange. Modern theories of air–sea momentum exchange over a wavy sea corroborate this assumption that surface features with longer wavelengths have little effect on momentum transfer. Donelan (1998), Makin and Kudryavtsev (1999), Kudryavtsev and Makin (2001), and Mueller and Veron (2009) all suggest, on theoretical grounds, that waves with wavelengths shorter than about 10 m or with wave numbers larger than order  $1 \text{ m}^{-1}$  support most of the air–sea momentum exchange.

Notice, if the limits in (4.1) were 0 to  $\infty$ , the integral would be the variance in surface elevation by definition. Hence,  $\xi^2$  is related to but smaller than the variance in surface roughness.

Andreas *et al.* (1993) investigated the surface elevation spectrum  $\Phi(\kappa)$  by analysing elevation profiles collected over sea ice in the Weddell Sea during the 1989 Winter Weddell Gyre Study. As a result, they recommended that future profiling lines intended for computing  $\Phi(\kappa)$  and the surface variance should be at least 255 m long with a sampling interval of 0.5 m or less. We implemented that sampling protocol on Ice Station Weddell for the purpose of relating  $z_0$  and  $\xi$ .

Figure 2 is one such levelling line surveyed on Ice Station Weddell. We made seven such profile lines during our deployment. The lengths varied – most were longer than the recommended 255 m – but the sampling interval was always 0.5 m. We made these levelling lines in the nominal upwind direction from the tower on which we were measuring  $u_*$  and tried to complete them during periods when the wind direction had been fairly constant.

Table I lists the statistics of these survey lines, the periods for which  $\xi$  can be associated with our  $z_0$  measurements, and

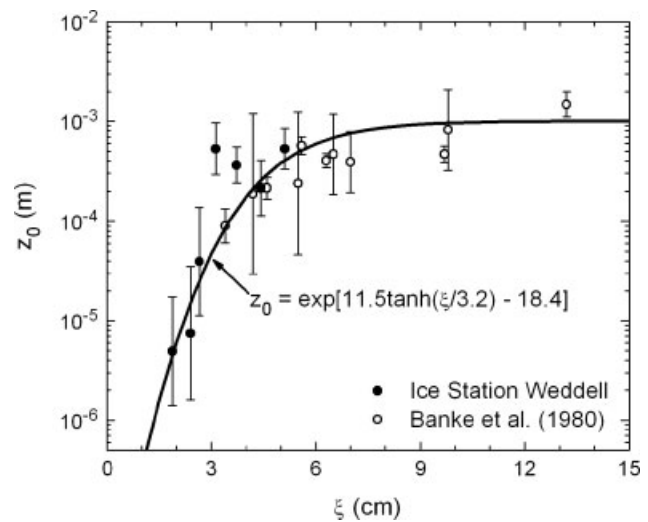


**Figure 3.** Average values of the aerodynamic roughness  $z_0$  and the associated physical roughness  $\xi$ , from (4.1), from measurements on Ice Station Weddell (Table I) and from the summary in Banke *et al.* (1980) (reanalysed in Table II). The error bars are  $\pm 2$  standard deviations in the geometric mean of  $z_0$ . The curve is (4.2).

mean measured values of  $z_0$  and  $C_{DN10}$  during these periods. In calculating these mean  $z_0$  and  $C_{DN10}$  values, I used data collected only when the hourly averaged wind direction was within  $\pm 50^\circ$  of the direction of the levelling line. The mean  $z_0$  values are calculated as the geometric mean because  $z_0$  values are approximately log-normally distributed (e.g. Vickers and Mahrt, 2006);  $C_{DN10}$  is calculated as the arithmetic mean. Because I have multiple measurements of  $z_0$  and  $C_{DN10}$  for each  $\xi$  value, I can also calculate error bars for these averages (not listed in Table I).

Banke *et al.* (1980) also presented a table like Table I (their Table 5). In it, however, they related the averaged  $z_0$  and  $C_{DN10}$  values through (3.3). That is, Banke *et al.* averaged only  $C_{DN10}$  (I think) and obtained the average of  $z_0$  through (3.3). Because  $z_0$  is approximately log-normally distributed while  $C_{DN10}$  is approximately normally distributed, their averages cannot be related through (3.3).

Fortunately, Banke and Smith (1973), Banke *et al.* (1976), and Banke *et al.* (1980) tabulated all the individual  $C_{DN10}$  values that went into the averages presented in Table 5 of Banke *et al.* (1980). Hence, I was able to recalculate mean  $C_{DN10}$  values and more reliable  $z_0$  values from the Banke and Smith (1973) and Banke *et al.* (1976, 1980) datasets. Table II reproduces Table 5 from Banke *et al.* (1980) with the new values. As important, from the individual  $C_{DN10}$  and  $z_0$  values, I was able to calculate error bars for the means; Banke *et al.* (1980) did not report these.

Figures 3 and 4 summarize the  $z_0$ ,  $C_{DN10}$ , and  $\xi$  data from Tables I and II. The Antarctic data from Ice Station Weddell are consistent with the Arctic data from Banke *et al.* (1980). My adding error bars to the Banke *et al.* values (not shown in their original plots) suggests how precise the measurements are and let me fit curves to the two datasets. That curve in Figure 3 is

$$z_0 = \exp\{11.5 \tanh(\xi/3.2) - 18.4\}, \quad (4.2)$$

where  $z_0$  is in metres and  $\xi$  is in centimetres.

Table I. Summary of the surface levelling surveys on Ice Station Weddell in 1992.

Profile ID	Measured on Julian day	Length (m)	Direction (°)	$\xi$ (cm)	Period Covered (UTC)	Count	$10^3 C_{DN10}$	$z_0$ (m)
Met-066	66	200.0	289	4.43	66.250–68.750	36	1.50	$2.15 \times 10^{-4}$
Met-069	69	300.0	174	5.11	68.833–69.542	16	1.69	$5.29 \times 10^{-4}$
Met-078	77–78	300.0	197	3.72	75.417–80.917	64	1.63	$3.62 \times 10^{-4}$
Met-097	95–96	292.5	180	2.40	95.292–98.417	7	0.845	$7.47 \times 10^{-6}$
Met-104	100	300.0	208	2.66	100.792–102.583	10	1.09	$3.94 \times 10^{-5}$
Met-110	110	204.5	294	3.13	107.875–112.292	55	1.85	$5.29 \times 10^{-4}$
Met-131	131	300.0	183	1.89	131.667–132.208	6	0.778	$4.94 \times 10^{-6}$

The ‘Period Covered’ identifies the turbulence sampling period for which the mean wind direction was within  $\pm 50^\circ$  of the survey line. ‘Direction’ is the azimuth, with respect to true north, of the survey line in the upwind direction from the instrument tower. ‘ $C_{DN10}$ ’ is the arithmetic mean of all good hourly values during this period; ‘ $z_0$ ’ is the geometric mean of all good values; ‘Count’ indicates the number of hourly samples used in the averaging.

Table II. A summary, with reanalysis, of the average  $C_{DN10}$  and  $z_0$  values reported in Table 5 of Banke *et al.* (1980).

Source	Identifier	$\xi$ (cm)	Count	$10^3 C_{DN10}$	$z_0$ (m)
Banke and Smith (1973)	Beaufort Sea AIDJEX 1971	5.6	2	1.68	$5.68 \times 10^{-4}$
	Beaufort Sea AIDJEX 1971	5.5	5	1.51	$2.38 \times 10^{-4}$
	Beaufort Sea AIDJEX 1972	9.8	2	1.82	$8.18 \times 10^{-4}$
	Beaufort Sea AIDJEX 1972	6.3	3	1.56	$4.03 \times 10^{-4}$
	Robeson Channel 1972	13.2	18	2.09	$1.48 \times 10^{-3}$
Banke <i>et al.</i> (1976)	Robeson Channel 1974	6.5	8	1.68	$4.68 \times 10^{-4}$
	Beaufort Sea AIDJEX 1975	4.6	6	1.39	$2.14 \times 10^{-4}$
	Flat AIDJEX 1975	7.0	4	1.57	$3.91 \times 10^{-4}$
	Hummocked AIDJEX 1975	9.7	2	1.61	$4.68 \times 10^{-4}$
Banke <i>et al.</i> (1980)	Beaufort Sea AIDJEX 1976	4.2	4	1.44	$1.88 \times 10^{-4}$
	Beaufort Sea AIDJEX 1976	3.4	4	1.19	$8.96 \times 10^{-5}$

The ‘Identifier’ corresponds with the description in Banke *et al.*; ‘Count’ is the number of individual measurements in the tabulated averages. As in Table I, ‘ $C_{DN10}$ ’ is the arithmetic mean, and ‘ $z_0$ ’ is the geometric mean.

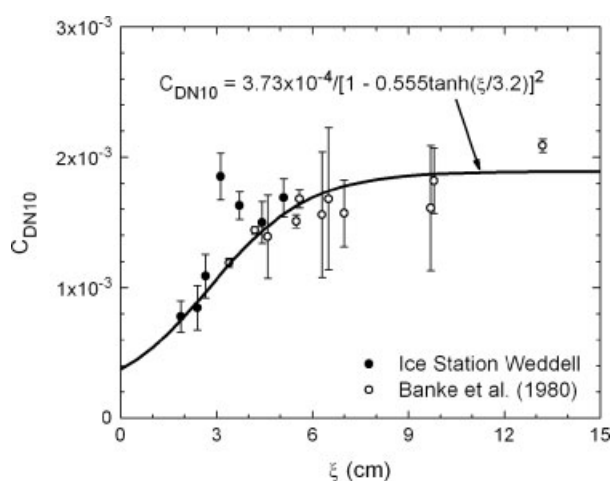


Figure 4. As in Figure 3, except this shows the arithmetic mean of  $C_{DN10}$ . The error bars are  $\pm 2$  standard deviations in this mean. The curve is (4.3).

To get the fitting curve in Figure 4, I simply transformed (4.2) using (3.3). The result is

$$C_{DN10} = \frac{3.73 \times 10^{-4}}{\{1 - 0.555 \tanh(\xi/3.2)\}^2} \quad (4.3)$$

Figures 3 and 4 do not include a lot of data for large physical roughness. Hence, in (4.2), I chose a hyperbolic tangent function to limit  $z_0$  at  $1.00 \times 10^{-3}$  m for large  $\xi$ . Likewise, (4.3) limits  $C_{DN10}$  to  $1.89 \times 10^{-3}$  for large  $\xi$ .

Figures 3 and 4 are a bit perplexing in light of Figure 1. The two panels in Figure 1 imply that the sea ice at Ice Station Weddell was generally more aerodynamically rough than the winter ice at SHEBA. Figures 3 and 4, in contrast, imply that the Arctic ice that Banke *et al.* (1980) observed was, generally, more physically and aerodynamically rough than the Antarctic ice at Ice Station Weddell. Admittedly, none of the Arctic data in Figures 3 and 4 are from SHEBA, so these comparisons are not exact.

Nevertheless, Figure 5 may provide an explanation for this puzzle. The top panel in Figure 5 includes all 866 hours of data for which measured  $z_0$  values and bulk  $u_*$  values were simultaneously available from Ice Station Weddell. That is, these are mostly the same data that went into the Ice Station Weddell panel in Figure 1. (I use the bulk  $u_*$  as the independent variable in Figure 5 to avoid the fictitious correlation that comes with using the measured  $u_*$  (Andreas *et al.*, 2010b)).

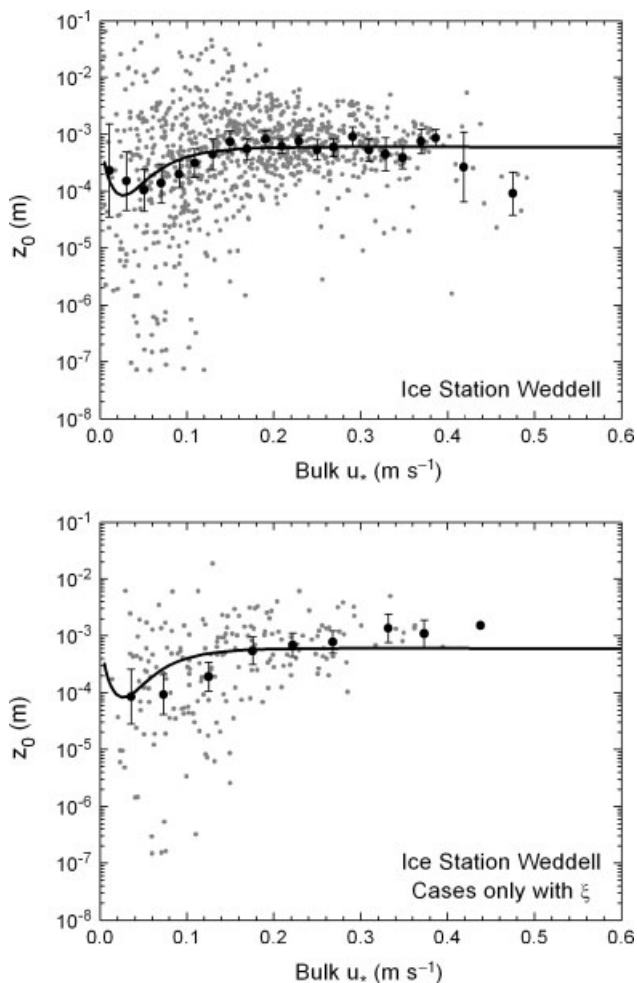


**Figure 5.** Hourly measurements of the aerodynamic roughness length  $z_0$  from (3.2) measured on Ice Station Weddell (grey circles) are plotted against the friction velocity  $u_*$  from the bulk flux algorithm described in section 2. The black circles are geometric mean values of  $z_0$  in  $u_*$  bins; the error bars are  $\pm 2$  standard deviations of the hourly points displayed. The curve in both panels is (2.4) with the Ice Station Weddell coefficient,  $B = 6.0 \times 10^{-4}$ . The top panel shows all 866 hours of Ice Station Weddell data; the lower panel shows just the 194 hours that coincided with measurements of the roughness metric  $\xi$ .

For only 194 hours, however, did we have  $z_0$  measurements and bulk  $u_*$  values from Ice Station Weddell that were well aligned with the survey lines that yielded the  $\xi$  values in Figures 3 and 4. The bottom panel in Figure 5 shows only these  $z_0$  values that coincided with the  $\xi$  measurements displayed in Figures 3 and 4.

The  $z_0$  values in the lower panel in Figure 5 tend to be smaller than in the full  $z_0$  set (top panel), especially for  $u_* < 0.15 \text{ m s}^{-1}$ , where almost 60% of the points in this panel lie. As a result, although the  $z_0$ – $\xi$  pairs in Figure 3 are accurate, they are not wholly representative of the sea ice at Ice Station Weddell. If we had been able to make more levelling surveys, we probably would have seen larger  $\xi$  values associated with the generally larger  $z_0$  values that we measured on Ice Station Weddell. In effect, additional  $\xi$  values from Ice Station Weddell would likely have been in line with the larger Arctic  $z_0$  and  $\xi$  values that Banke *et al.* (1980) obtained.

In summary, the roughness metric  $\xi$  is a reasonable candidate for the site-specific tuning parameter that I speculated about earlier. Figures 3 and 4 suggest that sea ice from the Arctic's central pack, from the Canadian

Archipelago, and from the Antarctic's central pack lies along a continuum in  $z_0$  and  $\xi$  space.

I thus speculate that the Arctic and Antarctic results in Figure 1 could not be represented by the same bulk flux algorithm because  $\xi$  values were different for the two locales. For the SHEBA sites,  $\xi$  probably tended to be 6 cm and less. For Ice Station Weddell, despite the biased sample presented in Figures 3 and 4,  $\xi$  probably ranged up to 9 cm or more.

## 5. Discussion

The ultimate goal of research along these lines is to infer the turbulent surface fluxes over sea ice from satellite remote sensing. Synthetic aperture radar (SAR) senses a backscatter signal that is related to the physical roughness of the surface. To close the analysis, we must relate aerodynamic roughness to physical roughness and then physical roughness to SAR backscatter.

Several groups have attempted to relate the SAR backscatter to the roughness of a surface. Greeley *et al.* (1988, 1991) and Blumberg and Greeley (1993) compared airborne SAR backscatter data to  $z_0$  values obtained from surface-layer measurements of the wind speed profile in arid regions. Rees and Arnold (2006) discussed relating satellite SAR data to the aerodynamic roughness of a glacier on Svalbard but did not actually measure the aerodynamic roughness – they estimated it from microtopography – nor were the SAR data coincident with their roughness measurements. Thus, to my knowledge, no one has completed the full sequence: aerodynamic roughness to physical roughness to satellite sensing of some surface roughness variable.

Figures 3 and 4 and Eqs (4.2) and (4.3) are now a good start to linking the aerodynamic roughness of sea ice to its physical roughness. Future work, however, needs the complete sequence: measurements of aerodynamic roughness coincident with measurements of physical roughness and SAR backscatter. Alternatively, in light of the relationships that Figures 3 and 4 summarize, we could also make progress on this problem if we had coincident measurements of physical roughness and SAR backscatter over sea ice.

## 6. Conclusions

Despite being based on 9000 hours of data collected over Arctic sea ice, the SHEBA bulk flux algorithm for winter (Andreas *et al.*, 2010b) was disappointing in its first test at predicting the surface stress over Antarctic sea ice. The modelled friction velocity,  $u_*$ , at Ice Station Weddell was biased low compared to eddy-covariance measurements of  $u_*$  (i.e. Figure 1). I concluded that a bulk flux algorithm for winter sea ice may need a site-specific parameter in its formulation of the aerodynamic roughness length,  $z_0$ .

This is, of course, not a new concept. Tables in Panofsky and Dutton (1984, p 123), Stull (1988, p 380), and Wieringa (1993), for instance, associate specific types of terrain with a typical value of aerodynamic roughness,  $z_0$ . Guest and Davidson (1991), in fact, present such a table specifically for sea ice and support it with photos of the surface. In essence, trying to associate  $z_0$  with a specific physical roughness has a long history.

On Ice Station Weddell, we measured the physical roughness of the snow surface for just this purpose: relating the physical roughness of a sea ice surface to simultaneous

measurements of  $z_0$ . This metric of physical roughness is  $\xi$  and derives from the integral of the spectrum of surface elevation over wave numbers from  $0.5 \text{ m}^{-1}$  to  $6.14 \text{ m}^{-1}$ , the Nyquist wave number.

Banke *et al.* (1980; cf. Banke and Smith, 1973; Banke *et al.*, 1976) had pioneered this type of analysis. Here, I recomputed the mean values of  $C_{DN10}$  and  $z_0$  that Banke *et al.* reported (Table II) to better account for the statistical properties of their individual measurements but also to deduce error bars for their measurements. Their set includes 58 individual measurements of  $C_{DN10}$  and  $z_0$  with coincident  $\xi$  values.

The Ice Station Weddell  $\xi$  data, reported here for the first time, more than quadruple the total number of  $C_{DN10}$ – $\xi$  and  $z_0$ – $\xi$  pairs we now have available for studying how the aerodynamic and physical roughness of sea ice are related. Moreover, Figures 3 and 4 show that the Banke *et al.* (1980) Arctic data and the Antarctic data from Ice Station Weddell constitute a continuum in  $C_{DN10}$ – $\xi$  and  $z_0$ – $\xi$  space. Consequently, the roughness metric  $\xi$  is a good candidate as a site-specific parameter for modelling the surface stress over sea ice surfaces.

The down side of  $\xi$  is that obtaining it is labour intensive; it is thus not readily available for modelling. I therefore recommended relating the aerodynamic roughness,  $z_0$ , to the physical roughness,  $\xi$ , as in Figure 3, and then relating this physical roughness to a remotely sensed variable – the backscatter from a satellite-borne SAR, for example. Creating this linkage is an important next step if we are to improve regional or global models that include sea ice.

### Acknowledgements

I would like to thank my colleagues in the SHEBA Atmospheric Surface Flux Group for help collecting, processing, and understanding the SHEBA data: Chris Fairall, Andrey Grachev, Peter Guest, Tom Horst, Rachel Jordan, and Ola Persson. I also thank the other members of the meteorology team on Ice Station Weddell for help collecting the data there: Kerry Claffey, Boris Ivanov, and Aleksandr Makshtas. I am grateful to an anonymous reviewer who provided comments that helped me better focus this story. The US National Science Foundation (NSF) supported this work with awards 06-11942 and 10-19322. NSF also supported my programmes on Ice Station Weddell and at SHEBA with previous awards.

### References

- Andreas EL. 1995. Air–ice drag coefficients in the western Weddell Sea. 2: A model based on form drag and drifting snow. *J. Geophys. Res.* **100**(C3): 4833–4843.
- Andreas EL. 2011. The fallacy of drifting snow. *Boundary-Layer Meteorol.*, submitted.
- Andreas EL, Claffey KJ. 1995. Air–ice drag coefficients in the western Weddell Sea. 1: Values deduced from profile measurements. *J. Geophys. Res.* **100**(C3): 4821–4831.
- Andreas EL, Lange MA, Ackley SF, Wadhams P. 1993. Roughness of Weddell Sea ice and estimates of the air–ice drag coefficient. *J. Geophys. Res.* **98**(C7): 12439–12452.
- Andreas EL, Fairall CW, Guest PS, Persson POG. 1999. 'An overview of the SHEBA atmospheric surface flux program.' Pp 411–416 in *Proceedings of Fifth Conference on polar meteorology and oceanography*, Dallas, Texas, 10–15 January 1999. American Meteorological Society: Boston.
- Andreas EL, Jordan RE, Makshtas AP. 2004. Simulations of snow, ice, and near-surface atmospheric processes on Ice Station Weddell. *J. Hydrometeorol.* **5**: 611–624.
- Andreas EL, Jordan RE, Makshtas AP. 2005. Parameterizing turbulent exchange over sea ice: The Ice Station Weddell results. *Boundary-Layer Meteorol.* **114**: 439–460.
- Andreas EL, Persson POG, Hare JE. 2008. A bulk turbulent air–sea flux algorithm for high-wind, spray conditions. *J. Phys. Oceanogr.* **38**: 1581–1596.
- Andreas EL, Horst TW, Grachev AA, Persson POG, Fairall CW, Guest PS, Jordan RE. 2010a. Parametrizing turbulent exchange over summer sea ice and the marginal ice zone. *Q. J. R. Meteorol. Soc.* **136**: 927–943.
- Andreas EL, Persson POG, Jordan RE, Horst TW, Guest PS, Grachev AA, Fairall CW. 2010b. Parameterizing turbulent exchange over sea ice in winter. *J. Hydrometeorol.* **11**: 87–104.
- Arya SPS. 1975. A drag partition theory for determining the large-scale roughness parameter and wind stress on the Arctic pack ice. *J. Geophys. Res.* **80**(24): 3447–3454.
- Banke EG, Smith SD. 1973. Wind stress on Arctic sea ice. *J. Geophys. Res.* **78**(33): 7871–7883.
- Banke EG, Smith SD, Anderson RJ. 1976. Recent measurements of wind stress on Arctic sea ice. *J. Fish. Res. Board Canada* **33**: 2307–2317.
- Banke EG, Smith SD, Anderson RJ. 1980. Drag coefficients at AIDJEX from sonic anemometer measurements. Pp 430–442 in *Sea ice processes and models*, Pritchard RS (ed). University of Washington Press: Seattle.
- Blumberg DG, Greeley R. 1993. Field studies of aerodynamic roughness length. *J. Arid Environ.* **25**: 39–48.
- Brunke MA, Zhou M, Zeng X, Andreas EL. 2006. An intercomparison of bulk aerodynamic algorithms used over sea ice with data from the Surface Heat Budget for the Arctic Ocean (SHEBA) experiment. *J. Geophys. Res.* **111**: C09001, DOI: 10.1029/2005JC002907.
- Donelan MA. 1998. Air–water exchange processes. Pp 19–36 in *Physical processes in lakes and oceans: Coastal and estuarine studies, volume 54*, Imberger J (ed). American Geophysical Union: Washington, DC.
- Fairall CW, Bradley EF, Rogers DP, Edson JB, Young GS. 1996. Bulk parameterization of air–sea fluxes for Tropical Ocean-Global Atmosphere Coupled-Ocean Atmosphere Response Experiment. *J. Geophys. Res.* **101**(C2): 3747–3764.
- Fairall CW, Bradley EF, Hare JE, Grachev AA, Edson JB. 2003. Bulk parameterization of air–sea fluxes: Updates and verification for the COARE algorithm. *J. Climate* **16**: 571–591.
- Garratt JR. 1992. *The Atmospheric Boundary Layer*. Cambridge University Press.
- Grachev AA, Andreas EL, Fairall CW, Guest PS, Persson POG. 2007. SHEBA flux–profile relationships in the stable atmospheric boundary layer. *Boundary-Layer Meteorol.* **124**: 315–333.
- Greeley R, Lancaster N, Sullivan RJ, Saunders RS, Theilig E, Wall S, Dobrovolskis A, White BR, Iversen JD. 1988. A relationship between radar backscatter and aerodynamic roughness: Preliminary results. *Geophys. Res. Lett.* **15**: 565–568.
- Greeley R, Gaddis L, Lancaster N, Dobrovolskis A, Iversen J, Rasmussen K, Saunders S, Van Zyl J, Wall S, Zebker H, White B. 1991. Assessment of aerodynamic roughness via airborne radar observations. *Acta Mech.* **2**: (Suppl.): 77–88.
- Guest PS, Davidson KL. 1991. The aerodynamic roughness of different types of sea ice. *J. Geophys. Res.* **96**(C3): 4709–4721.
- Horst TW, Oncley SP, Semmer SR. 1997. 'Measurement of water vapor fluxes using capacitance RH sensors and cospectral similarity.' Pp 360–361 in *Proceedings of 12th Symposium on boundary layers and turbulence*, Vancouver, British Columbia, 28 July–1 August 1997. American Meteorological Society: Boston.
- Kudryavtsev VN, Makin VK. 2001. The impact of air–flow separation on the drag of the sea surface. *Boundary-Layer Meteorol.* **98**: 155–171.
- Lettau H. 1969. Note on aerodynamic roughness–parameter estimation on the basis of roughness–element description. *J. Appl. Meteorol.* **8**: 828–832.
- Makin VK, Kudryavtsev VN. 1999. Coupled sea surface–atmosphere model. 1: Wind over waves coupling. *J. Geophys. Res.* **104**(C4): 7613–7623.
- Militzer JM, Michaelis MC, Semmer SR, Norris KS, Horst TW, Oncley SP, Delany AC, Brock FV. 1995. 'Development of the prototype PAM III/Flux-PAM surface meteorological station.' Pp 490–494 in *Proceedings of 9th Symposium on meteorological observations and instrumentation*, Charlotte, North Carolina, 27–31 March 1995. American Meteorological Society: Boston.
- Mueller JA, Veron F. 2009. Nonlinear formulation of the bulk surface stress over breaking waves: Feedback mechanisms from air–flow separation. *Boundary-Layer Meteorol.* **130**: 117–134.
- Overland JE. 1985. Atmospheric boundary layer structure and drag coefficients over sea ice. *J. Geophys. Res.* **90**(C5): 9029–9049.

- Panofsky HA, Dutton JA. 1984. *Atmospheric Turbulence: Models and Methods for Engineering Applications*. John Wiley and Sons: New York.
- Paulson CA. 1970. The mathematical representation of wind speed and temperature profiles in the unstable atmospheric surface layer. *J. Appl. Meteorol.* **9**: 857–861.
- Persson POG, Fairall CW, Andreas EL, Guest PS, Perovich DK. 2002. Measurements near the Atmospheric Surface Flux Group tower at SHEBA: Near-surface conditions and surface energy budget. *J. Geophys. Res.* **107**: 8045, DOI: 10.1029/2000JC000705.
- Raupach MR. 1992. Drag and drag partition on rough surfaces. *Boundary-Layer Meteorol.* **60**: 375–395.
- Rees WG, Arnold NS. 2006. Scale-dependent roughness of a glacier surface: Implications for radar backscatter and aerodynamic roughness modelling. *J. Glaciol.* **52**: 214–222.
- Shao Y, Yang Y. 2005. A scheme for drag partition over rough surfaces. *Atmos. Environ.* **39**: 7351–7361.
- Stull RB. 1988. *An Introduction to Boundary Layer Meteorology*. Kluwer: Dordrecht.
- Vickers D, Mahrt L. 2006. Evaluation of the air–sea bulk formula and sea-surface temperature variability from observations. *J. Geophys. Res.* **111**: C05002, DOI: 10.1029/2005JC003323.
- Wieringa J. 1993. Representative roughness parameters for homogeneous terrain. *Boundary-Layer Meteorol.* **63**: 323–363.